https://doi.org/10.1038/s44328-025-00057-8

Organic electrolyte gated field effect transistor for detecting alpha synuclein longitudinally in Parkinsonism mouse model

Srishti Johri[1,5], Dennis Chan[2,5], Roslyn S. Massey[3], Daniel Knight[4], Maria C. DeRosa[4], Matthew R. Holahan[2] & Ravi Prakash[1] ✉

Parkinson's Disease (PD) is an age-progressive disorder caused by misfolding of alpha-synuclein (α-Syn) that can begin years before clinical symptoms appear, making early diagnosis crucial for timely intervention. In this study, a novel antibody-functionalized Organic Electrolyte-Gated Field-Effect-Transistor (Ab-OEGFET) biosensor was implemented to detect α-Syn levels in blood serum samples from an A53T Transgenic (TG) mouse line. PD-like pathology was examined in blood serum using Ab-OEGFET devices and in brain tissue samples using Western Blot and immunohistochemistry. Different forms (monomeric, phosphorylated, oligomeric) of α-Syn were identified in low volumes of blood serum samples collected from TG and Wild Type (WT) populations of mice at ages 2, 5 and 8 months, and the biosensor response was correlated to Blot and immunohistochemistry results. The Ab-OEGFETs performance in this study is a promising result towards a minimally invasive blood biomarker-based multianalyte testing strategy for early screening of PD and similar neurodegenerative disease pathologies.

Alpha-synuclein (α-Syn) aggregation is a hallmark of Parkinson's disease (PD), driven by the pathological accumulation of misfolded α-Syn protein that contributes to neuronal loss and the onset of motor symptoms such as bradykinesia, resting tremor, and rigidity[1]. While the majority of PD cases are sporadic, mutations in the *SCNA* gene, such as A53T, have been linked to familial forms of PD, highlighting the role of α-Syn in PD pathology[2]. By the time PD is clinically diagnosed, up to 80% of dopaminergic neurons in the substantia nigra pars compacta (SNc) are already lost[3]. This extensive neuronal damage limits therapeutic options, which largely focus on symptom management rather than addressing underlying mechanisms[4]. These challenges underscore the critical need for early detection methods to identify pathology during the preclinical phase.

The A53T transgenic mouse line expresses the human A53T mutation associated with familial PD[5] and has been widely utilized to study PD pathology[6,7]. This mutation of α-Syn is strongly linked to increased phosphorylated α-Syn (pα-Syn), with studies showing nearly 90% of α-Syn aggregates are phosphorylated compared to normal brain conditions[8]. This Parkinsonism model recapitulates key aspects of PD progression, including age-dependent α-Syn aggregation, accumulation of pα-Syn[9], and motor deficits[6,10,11]. A53T mice exhibit an early accumulation of α-Syn, which progresses to insoluble fibrils in the gut and ultimately leads to neurodegeneration in the central nervous system (CNS)[7,8,12]. The presence of pα-Syn, a pathological biomarker of PD, also appears early in A53T mice, prior to the onset of motor symptoms[11]. Due to its robust α-Syn pathology, the A53T model serves as a valuable tool for testing novel diagnostic approaches that monitor α-Syn misfolding and aggregation.

Recent advances in fluid biomarker-based diagnostic methods for PD focus on detecting pathogenic α-Syn species before neurodegeneration occurs; however, most methods, such as the α-Syn seed amplification assays (α-Syn-SAA) rely on cerebrospinal fluid (CSF) collection, which is highly invasive[13]. Over the past few decades, multiple less invasive and point-of-care (POC) ready approaches have been introduced and investigated using fluid biomarkers and diagnostic techniques[14,15]. This includes label-free electrochemical biosensors, which combine immunoassays with electrochemical sensing, for various diseases, including PD and cancer[16,17], and electrolyte-gated transistor structures such as organic electrochemical

[1]Department of Electronics Engineering, Carleton University, Ottawa, ON, Canada. [2]Department of Neuroscience, Health Sciences Building, Carleton University, Ottawa, ON, Canada. [3]Dept. of Mechanical Engineering, Stanford University, 418 Panama Mall, Stanford, CA, USA. [4]Department of Chemistry and Institute of Biochemistry, Carleton University, Ottawa, ON, Canada. [5]These authors contributed equally: Srishti Johri, Dennis Chan. ✉e-mail: RaviPrakash@cunet.carleton.ca

transistor (OECT)[18,19] and electrolyte-gated organic field effect transistor (EGOFET)[20,21], for transducing biological and biochemical signals from protein biomarkers into label-free electronic parameters. An approach for detecting protein biomarkers such as immunoglobulins has been explored using OECT by Macchia et al.[19], while a strategy to quantify total α-Syn in spiked buffer solution has been explored using EGOFET devices by Ricci et al.[20]. Major challenges with these POC sensors for detecting protein aggregation in complex biofluids include poor specificity and selectivity in the presence of serum albumin, limitations to sensing range due to misfolding, and broad variation in protein sizes due to oligomerization, and pseudo-capacitance arising from electrode-electrolyte or electrolyte-semiconductor interactions. In our prior work[22], Massey et al. demonstrated a label-free organic electrolyte-gated field effect transistor (OEGFET) aptasensor, which exploited the target-specific binding of protein molecules to aptamers immobilized within the sensor's soft-fluidic microchannel. The apta-OEGFET biosensor detected α-Syn levels in spiked saliva samples, demonstrating the platform as a label-free, POC-ready sensor for protein biomarkers. The OEGFET platform was subsequently modified to incorporate different antibody surface immobilization, and the resultant antibody-OEGFET (Ab-OEGFET) devices were evaluated, alongside the apta-OEGFET for measuring two protein biomarkers, α-Syn and beta-amyloid, in spiked samples of serum collected from healthy mice[23,24].

The reported study is a significant step towards fully realizing the Ab-OEGFET device as a minimally invasive PoC platform for detecting less invasive fluid biomarkers of PD and other neurodegenerative diseases. We present an Ab-OEGFET device architecture optimized to accommodate multiple antibodies immobilized individually across the device array, to investigate different formations of the α-Syn protein. A large number of device prototypes were deployed in a longitudinal transgenic mouse model evaluation study spanning over 8-months. The study investigated changes in blood serum protein levels of different α-Syn formations and compared their presence in blood serum to brain tissue samples. An A53T transgenic (TG) mouse model was deployed to study disease progression with animals tested at 2-, 5- and 8-months stages, along with age-matched wild type (WT) controls. The Ab-OEGFET device responses were analyzed using three different antibody candidates across serum dilution series in several animals from each age group to establish sensing range, optimal device operating point, and optimal sensor biasing conditions. To analyze the performance of selected antibody candidates and to compare serum protein levels to their presence in brain tissue, Western Blot quantification and immunohistochemical detection were implemented on brain tissue samples collected in tandem with the serum samples. Ab-OEGFET biosensor performance across the longitudinally collected TG mice serum was then correlated to Western Blot quantification in brain tissue.

Results

Figure 1A, B shows the rendering of the Ab-OEGFET sensor assembly with a soft-integrated microfluidic channel, whereas the sensor fabrication and testing is displayed in Fig. 1C–E and detailed in the Methods section. The Ab-OEGFET sensing behavior, shown in Fig. 2, was evaluated using Marinov model-based organic transistor device parameter extraction strategy, with the device biased in a desired operating range that includes linear and early saturation region of the transistor (Fig. 2A, B)[22]. A similar principle has been utilized in our prior studies, where the effective utilization of extracted parameters is explained for the sensor device model[22]. In essence, the OEGFET device holds a top-gate orientation, with a soft microfluidic channel sandwiched between the top gate, the OSC layer, and two thin film soft polymer layers. Each polymer layer within the device cross-section acts as a dielectric layer and contributes towards the effective gate-to-channel capacitance (Fig. 1B); this is cumulatively expressed as a lumped dielectric layer ($\hat{C}_{di}$), explained as capacitors connected in series.

The electrolytic solution in the microfluidic channel contributes additional capacitance terms ($\hat{C}_{\text{electrolyte}}$) to the dielectric layer's overall output, with the dominant contribution arising from the charge transfer and surface binding layer capacitance terms[17]. The sensor response shown in Fig. 2C is an inverse modulation of device current with analyte concentration when surface binding effects dominate over bulk electrolytic terms, i.e., matrix effect. This is identified as the sensing region. For a device in sensing region, the α-Syn concentration in serum samples governs the protein-to-antibody binding inside the microfluidic channel, which affects $\hat{C}_{di}$ via the efficient formation of EDL and charge transfer capacitance, modulating the production of the device saturation current (ID-SAT) as the

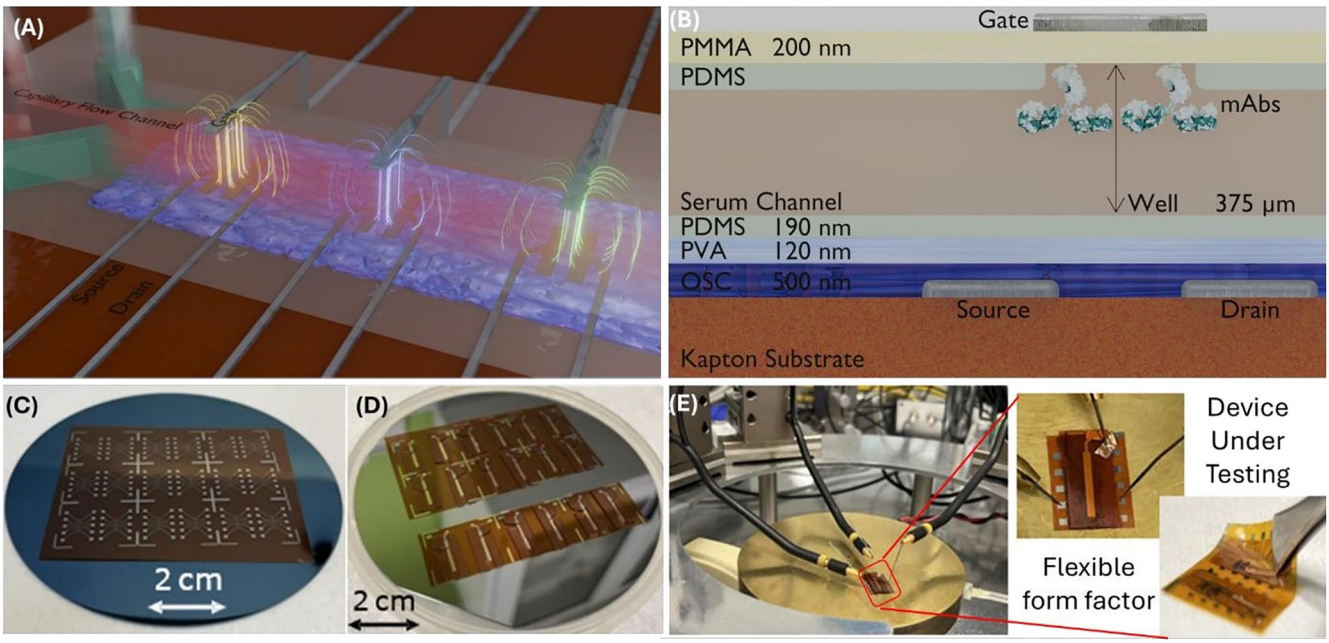

Fig. 1 | Rendered diagrams and snapshots showing the Ab-OEGFET device concept, and fabrication and testing process. A Illustration showing the soft channel integrated Ab-OEGFET Biosensor, **B** cross-section of the Ab-OEGFET device showing solid, electrolytic, and bio-functional layers, **C**, **D** array of metal source-drain and gate electrode on Kapton, **E** fully assembled device under testing with serum in a microchannel.

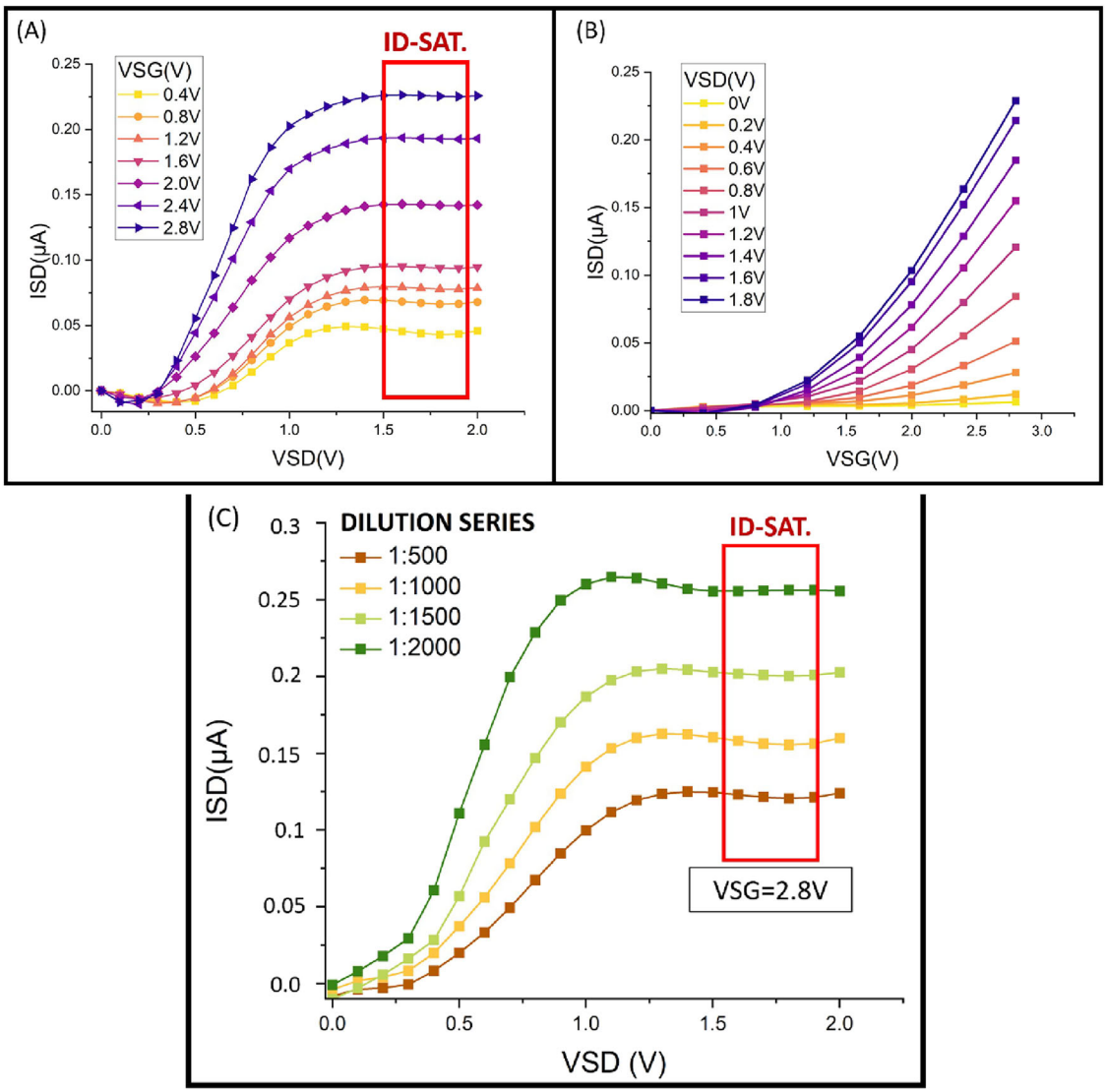

Fig. 2 | Ab-OEGFET device response curves. The I-V output (**A**) and transfer (**B**) curves were obtained from normalized-fitted data via device tested with stable buffer predicting threshold voltage (1.0 to 1.2 V) from transfer curve and saturation region of 1.5–2.0 V (ISD) from output curve. **C** Device output characteristics **(unfiltered)** collected from a dilution series of an 8-month TG serum sample. ISD Source to Drain Current, VSD Source to Drain Voltage, VSG Source to Gate Voltage, & ID-SAT Saturated Drain Current.

sensor output (Fig. 2C). In this study, changes in ID-SAT, as exhibited by the device per serum sample under fixed applied gate voltage, were used as the device data to visualize sensitivity.

Ab-OEGFET targeting total monomers & oligomers α-Syn in blood serum

The Ab-OEGFET immobilized with monomer total-specific antibodies (Anti-α Syn, clone 2F12) in the microfluidic channel was first investigated for its specificity towards the targeted biomarker, total α-Syn monomer. Immobilization of antibodies within the microfluidic channel was characterized using fluorescent microscopy (Supplementary Fig. 1). Binding of monomers exclusively is a challenging process due to the agglutination property of proteins in serum, which leads to the formation of larger complexes that may encapsulate the epitope for Ab-Ag binding. Hence, testing was performed by keeping the preventive measures under consideration. The investigation used blood serum samples from three different age groups of mice: 2-, 5-, and 8-months[25,26]. Serum was extracted from TG and WT mice from each age group to visualize changes in the concentration of biomarkers across the longitudinally collected samples.

The Ab-OEGFET technology was demonstrated in an early-stage by Johri et al., [23], as sensitive to spiked biomarker levels in diluted WT mice serum samples. The present study focused on the device's behavior when targeting multiple forms of α-Syn protein across different age group mice serum samples. It was therefore imperative to use serum dilution series from samples across all age groups to analyze the challenges in dealing with different blood serum samples and the composition of proteins and other biomolecules, which can interfere with the efficiency of antibody binding (Supplementary Fig. 9).

In this investigation, the first batches of Ab-OEGFET devices were fabricated with immobilized antibody targeting total α-Syn monomer, and the devices tested on serum samples from the three age groups. As shown in Fig. 3 (left), the first tested data series of monomeric α-Syn in a serum sample from 2-month-old mice for the gate bias -2.8 V showed a narrow range of sensing region in the TG age group and achieved inflection in signal intensity at the same concentration compared to WT. The decreasing current with increasing concentration represents the formation of an antibody-protein biomolecule complex layer with increasing concentration[14]. Extremely low output current from the biosensor was

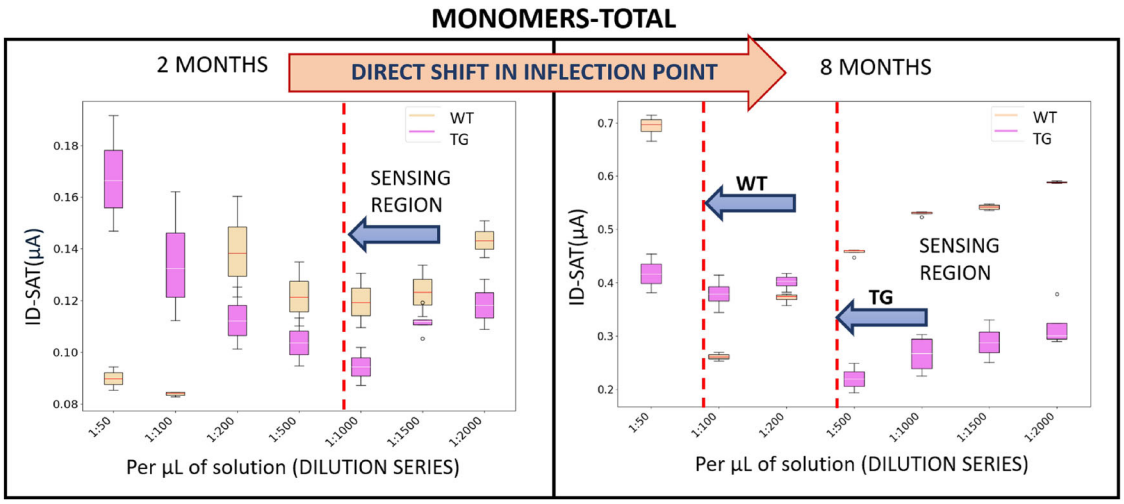

Fig. 3 | Ab-OEGFET device response to longitudinal variation of total monomeric α-Syn in dilution series samples. (Left) Data targeting monomer total α-Syn in blood serum dilution series in TG and WT dilution series (mean value of all replicates tested per age group) at 2months and at 8 months (Right); *ID-SAT* Device output current in saturation region; Left side of red marker line represents Matrix region.

expected to show no EDL formation, meaning no sensing. However, when a similar serum sample (2 months old) was tested with another set of devices immobilized with anti-oligomer-specific α-Syn antibodies, there was a comparatively broader sensing region. When monomer oligomerizes, the formation of efficient EDL is affected and is explained by the clumping of protein within serum samples.

In the second set of experiments done with 5-month-old serum samples for monomeric and oligomeric biomarkers, a change in the intensity of the signal was observed. Oligomers are larger and result in unproportionate or no formation of EDL, which explains improper binding. The concentration of the solution causes current modulation, and the biosensor responds via the effective binding of biomolecules. The presence of big clumps due to agglutination or oligomeric chunks affects the overall device response. In the third set of experiments with 8-month-old serum samples for monomeric and oligomeric biomarkers, the shift in the inflection point was visible for both protein morphologies (Figs. 3, 4). The oligomers achieved matrix effect at early dilution (8-month data in Figs. 3, 4) because of the larger size biomolecules that covered more surface area at an early pace. On the contrary, monomers of comparatively smaller size and higher concentration are believed to develop uniform EDL and high-intensity signal.

In summary, the Ab-OEGFET correctly predicted the correlation between device response and the biomarker concentration in dilution series for each age group, as shown in Figs. 3 and 4. The significant values of ID-SAT/ signals received from the device established an inverse correlation with biomarker concentration in the working solutions of serum samples. The inverse correlation facilitated the detection of biomarkers present in lower concentrations of diluted serum solutions. To visualize the specificity of the device, a set of OEGFETs were functionalized with anti-GFP antibodies and tested them using 8-month serum samples from both wild-type (WT) and transgenic (TG) animals. As expected, neither group exhibited significant signal responses within the sensing region. Current drop was observed at lower dilutions explaining no binding within the channel and higher concentration of the serum. This result confirms that the observed device sensitivity is specific to the interaction between the immobilized antibody and its target biomarker, and not due to nonspecific serum effects or device artifacts (Fig. 4B).

Aptamer-OEGFET Targeting Monomeric α-Syn in Blood Serum

In assessing suitable recognition molecules for different forms of α-Syn in our animal model study, we investigated the performance of aptamer-based OEGFET devices for the feasibility of combining two recognition molecules within a single sensor footprint. We have recently compared the performance of our α-Syn selective aptamer[27] against antibodies for detecting changes in total α-Syn monomer in different fluid matrices. The aptamer-based device platform uses non-covalently immobilized α-Syn aptamers as bio-recognition molecules (Supplementary Figs. 2, 3)[24]. To assess the aptamer-based OEGFET sensor, a similar set of dilution series was performed to compare the best-attained sensitivity with blood serum. The evaluation was aimed at examining whether the excellent sensing range of aptamer-based devices reported previously in spiked saliva and serum matrix samples was transferable to serum samples with high analyte and background protein concentrations. The entire longitudinal array of experiments was performed at −2.4 V gate bias and drain to source voltage at −3.0 to −3.5 V; the summary plots are reported in Fig. 5.

The aptamer-based OEFGET demonstrated an inverse device response to decreasing serum protein concentrations (i.e., higher device current for higher serum dilutions in the sensing range), however, a few new observations were evident. The resolution of aptamer-based device response was far lower than Ab-OEGFETs and the response suffered more in TG samples where higher concentrations of monomer α-Syn were anticipated and demonstrated by the newly designed Ab-OEGFET devices. In 2-month WT, the device showed a periodic drop in the sensing region, whereas in 2-month TG samples inflection point arising from matrix effect shifted to a higher concentration, providing an expanded sensing range. Hence, it explains that aptamer-based OEGFETs suffered due to high concentrations of analyte and impacted the device performance.

The serum matrix effect plays a major role in establishing the cut-off for the aptamer-based sensor's sensing region. As observed in Fig. 5, the aptamer-OEGFET did not predict a repeatable trend in matrix effect when tested with dilutions of TG serum samples across age groups. In a 2-month sample (Fig. 5A, B), no defined matrix effect was observed in TG compared to WT. The device only showed an abrupt inflection point for one dilution (1:500) with 5-month-old TG serum samples, followed by a continued inverse concentration response (Fig. 5C, D). In 8-month-old TG mice serum samples (Fig. 5E, F), the matrix effect was quite visible, but device sensitivity was highly unpredictable. Based on these observations, it was established that the previous generation Aptamer-OEGFET in its current form factor is not a reliable platform for tracking α-Syn biomarkers in clinically relevant concentration ranges, such as the current animal model study.

Increased α-Syn monomer in A53T transgenic mice across age

Western blot analysis of α-Syn monomer from the motor cortex revealed a significant interaction between age and genotype ($F_{(2,30)} = 8.71$, $p < 0.05$) with a significant elevation in α-Syn monomer protein in A53T TG mice

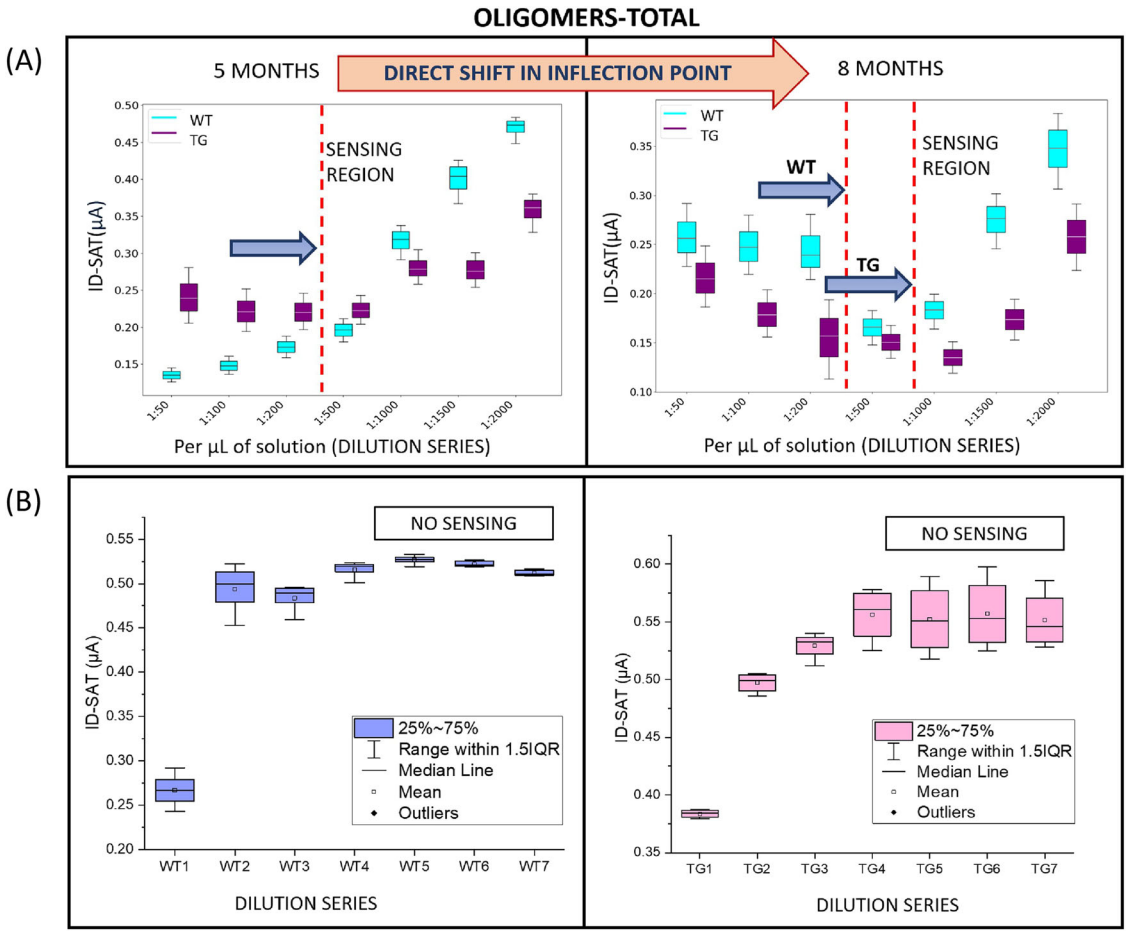

Fig. 4 | Ab-OEGFET device response to longitudinal variation of total oligomeric α-Syn in dilution series samples, compared to a control device set with anti-GFP antibody. A Sensor data against total oligomeric α-Syn in blood serum dilution series in TG and WT dilution series, 2 months (Left) and 8 months (Right); ID-SAT= Device output current in saturation region; Left side of Red marker line represents Matrix region; **B** Anti-GFP Ab-OEGFET data showing no sensitivity when tested with 8-month old WT and TG serum samples; Dilution series from WT1 to WT7 and TG1 to TG7 are 1:50, 1:100, 1:200, 1:500, 1:1000, 1:1500, 1:2000.

compared to WT controls ($F_{(1,30)} = 589.26$, $p < 0.05$), indicating that the A53T mutation is associated with higher levels of α-Syn monomers (Fig. 6A and B)[5]. There was also a main effect of age ($F_{(2,30)} = 12.84$, $p < 0.05$), with post hoc analysis showing more α-Syn monomer levels in the 8-month-old group compared to the 2- and 5-month-old groups (Fig. 6B). These results are consistent with other reports, as mutations in α-Syn increase protein levels compared to non-transgenic animals[6] and that α-Syn expression increases with age[28].

To assess α-Syn oligomeric accumulation, Western blot analysis with the Syn33 antibody (Fig. 6A) revealed a significant main effect of genotype, with higher levels of oligomeric α-Syn in the motor cortex of TG mice compared to age-matched controls ($F_{(1,30)} = 9.765$, $p < 0.05$). There was also a main effect of age, with older mice having higher levels of oligomeric α-Syn compared to younger mice ($F_{(2,30)} = 15.18$, $p < 0.05$). No significant difference was observed between 2- and 5-month TG groups (Fig. 6B), but a notable increase was detected between 5- and 8-month TG groups ($p < 0.05$). WT mice also exhibited elevated oligomeric α-Syn, as 8-month mice had significantly higher levels than 2-month mice ($p < 0.05$), suggesting that aging alone can contribute to α-Syn aggregation[29]. Although WT mice lack the A53T mutation, 8-month mice displayed similar levels of oligomeric α-Syn compared to 2- and 5-month TG mice ($p > 0.05$), which is in line with other studies that suggest that the formation of toxic α-Syn species can be present under normal physiology[30,31]. The rise in oligomeric α-Syn in TG mice between 5- and 8 months is consistent with prior studies demonstrating that the A53T mutation promotes α-Syn misfolding and enhances oligomerization which increases with age[10]. The interaction between age and genotype was not significant ($p > 0.05$) which may indicate the slow progression of pathology in the heterozygous model over time compared to accelerated α-Syn pathology in homozygous models[10].

Consistent with the Western blot findings, a similar age-dependent response was observed in the Syn33 Ab-OEGFET devices where a more demonstrable inverse current to concentration modulation was present in samples from age group 5- and 8-months (Fig. 4). The device behavior shift also showed less of a differential between the WT serum samples and TG serum samples at various age groups, which is similarly observed in the Blot data of Fig. 6. Literature indicates the possibility of lack of binding specificity between the Syn33 antibody and different α-Syn polymeric formulations[32]. This could explain an improved trend from 5- to 8-months when oligomeric form is more dominantly present.

Increased expression of pα-syn in transgenic mice with the A53T mutation

Phosphorylated α-Syn (pα-Syn) serves as a marker of pathogenic α-Syn aggregation[33]. Given the observed increase in αSyn monomer and oligomer levels in TG mice, we examined pα-Syn in the motor cortex using Western blot. As shown in Fig. 7A, B, TG mice exhibited a significant increase in pα-Syn expression compared to WT controls ($F_{(1,30)} = 48.76$, $p < 0.05$), indicating that the A53T mutation accelerates α-Syn pathology[9]. A significant interaction between genotype and age was found ($F_{(2,30)} = 4.2577$, $p < 0.05$), suggesting that elevated pα-Syn in the TG group increases with age[11]. Although no significant differences in pα-Syn levels were observed between 2- and 5-month-old TG groups, a significant increase in pα-Syn expression

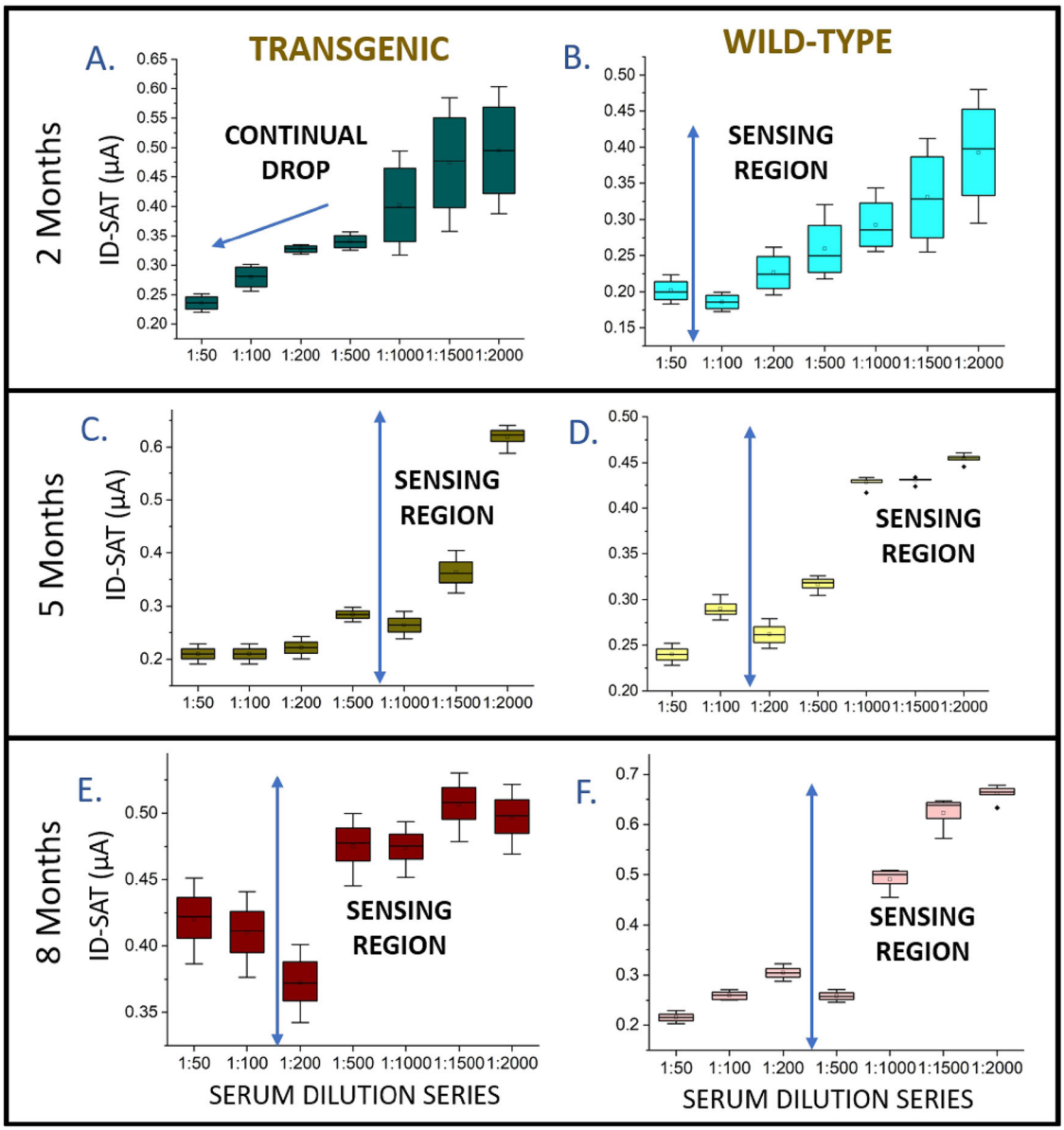

Fig. 5 | Aptamer-OEGFET device data targeting monomer α-Syn in blood serum dilution series in TG and WT samples. Dilution series results for **A**, **B** 2 months, **C**, **D** 5 months, **E**, **F** 8 months. ID-SAT Device output current in saturation region.

was detected between 5- and 8-month-old TG groups ($p < 0.05$). This pattern of increased pα-Syn expression aligns with the previous finding of the progressive accumulation of α-Syn oligomers (Fig. 6B). Given that the A53T mutation drive the overexpression of α-Syn, elevated levels of oligomeric α-Syn may promote a greater tendency for the protein to become phosphorylated with age.

Immunohistochemical detection of pα-Syn in the motor cortex

Immunohistochemical detection of pα-Syn staining in the motor cortex revealed a significant interaction between genotype and age ($F_{(2,30)} = 141.59$, $p < 0.05$). A main effect of genotype revealed more pα-Syn-positive cell counts in TG groups compared to WT controls ($F_{(1,30)} = 1085.94$, $p < 0.05$). A significant effect of age was also observed ($F_{(2,30)} = 146.18$, $p < 0.05$), with the 8-month-old group showing more pα-Syn staining than the 2- and 5-month-old groups Fig. 8.

Comparative Analysis of pα-Syn in Ab-OEGFET and Western Blot

Based on the sensor data from the serum dilutions (Figs. 3 and 4), and the Western Blot data (Figs. 6 and 7), anti pα-Syn antibody was selected as the optimal antibody to correlate sensor performance with serum samples to the Blot data and to quantify the pα-Syn concentration across the different age groups. As seen in Fig. 9A, the normalized sensor data from WT serum depict no defined changes in signal intensity and exhibits high ID-SAT values that explain the predictable low levels of pα-Syn concentration across all WT samples. Device data also exhibit a significant drop in current between WT and TG samples at all age groups, starting at 2-months, which indicates that the sensor could detect low threshold levels of pα-Syn in serum samples at an early stage.

Upon comparing the sensor response to Western Blot quantification of pα-Syn (Fig. 9B), the Western Blot data show an increase in normalized signal intensity from 2 to 8- months, indicating an increase in pα-Syn concentration in the age range tested. The device provided the highest current intensity in the 2-month-old group (sample with the lowest concentration of pα-Syn) and the lowest current intensity in the 8-month-old sample (sample with the highest concentration of pα-Syn). The signal drop in TG from 2 to 8-month serum samples clearly demonstrates an increasing concentration of pα-Syn with age in the A53T mice.

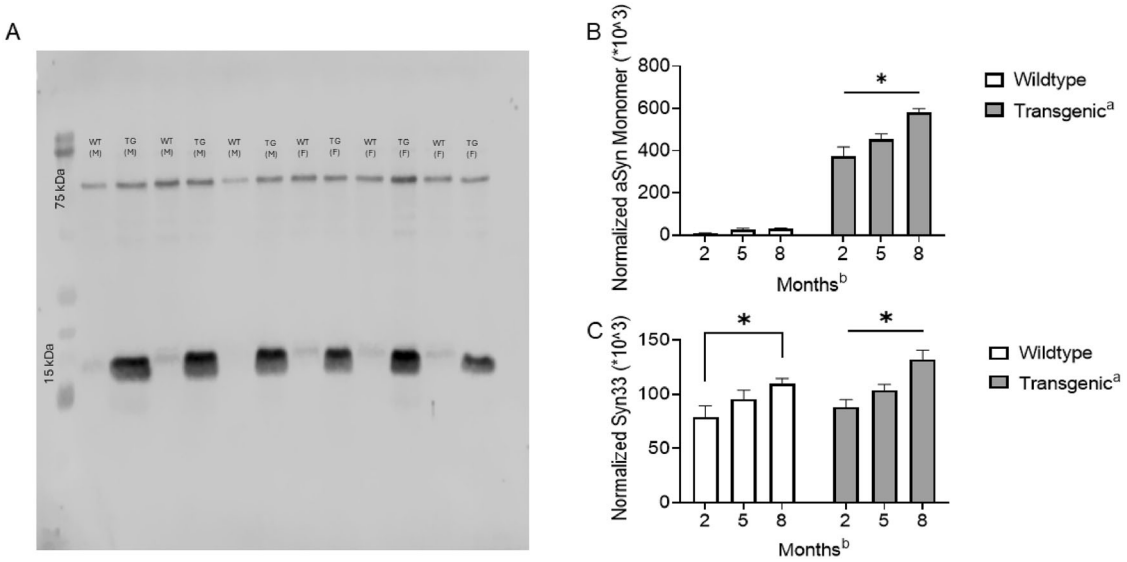

Fig. 6 | Western blot images and data for α-Syn monomer and α-Syn oligomer. **A** α-Syn monomer (15 kDa) and α-Syn oligomers (75 kDa) levels in 8-month-old animal models. **B** Western blot data targeting monomeric α-Syn levels in TG and WT mice. **C** Western blot data targeting oligomeric α-Syn levels in TG and WT mice. Data are presented as mean ± SEM. The asterisk indicates higher levels of monomeric and oligomeric forms of α-Syn in the 8-month TG group compared to the 2- and 5-month TG groups, $p < 0.05$. 'a' denotes a significant main effect of genotype (TG vs WT); 'b' denotes a significant main effect of age.

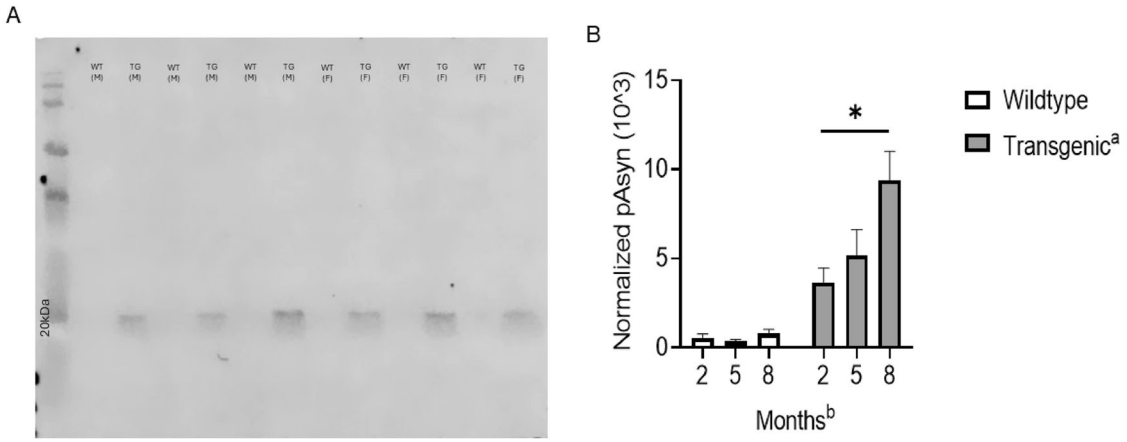

Fig. 7 | Western blot of pα-Syn levels. **A** Western blot representation of 8-month TG and WT mice. **B** Western blot data targeting pα-Syn levels in TG and WT mice. Data are presented as mean ± SEM. The asterisk indicates higher levels of pα-Syn in the 8-month TG group compared to the 2- and 5-month TG groups, $p < 0.05$. 'a' denotes a significant main effect between genotypes (TG vs WT); 'b' denotes a significant main effect of age.

To demonstrate this increase in pα-Syn compared to levels of total α-Syn monomers, the current modulation response from the two different device sets was transformed in a ratio plot depicting the normalized ID-SAT ratio between the pα-Syn and α-Syn mono Ab-OEGFET devices for the same serum samples. As shown in Fig. 9C, the ratio of pα-Syn over α-Syn monomer strongly shows that a multianalyte Ab-OEGFETs device clearly differentiates pathological progression in TG mice with age as early as two-month, confirming its suitability as an early detection platform.

Finally, to provide additional insight into levels of pα-Syn in serum detected by the sensor and in brain using Western Blot, and to correlate sensor performance to Blot testing longitudinally, Pearson Correlation Coefficient (r) was calculated across the different ages (Fig. 9D). Concentrations of pα-Syn in the motor cortex as evident in Blot data and concentration of pα-Syn in serum as detected by the sensor device were strongly negatively correlated and statistically significant, $r = -0.95$, $p < 0.001$. These observations confirm the inverse correlation in sensor signal intensity in serum to the Blot data in brain tissue samples, which evidently indicates an increase in serum concentration levels of pα-Syn aligning well with increased concentration in the brain tissue.

The strong correlation between serum sensor data and brain tissue Blot data is vital because it validates the sensor's ability to detect early indications of PD pathology progression directly in serum. This is a vital demonstration that the sensor can not only capture small, low-concentration variability of analyte in serum samples, but it can furthermore distinguish small longitudinal changes in analyte concentration, which can be used to infer disease progression or the effect of novel therapeutics. This behavior is beneficial for the device to capture a larger range of biomarker concentrations related to PD and other neurodegenerative diseases. This is the first time this has ever been shown for an early-stage point-of-care-ready biosensor technology, and it highlights the usability of the device to detect pα-Syn in serum that matches pathological progression in the brain.

The experimental validation of the Ab-OEGFET device using Western Blot demonstrates a reliable and sensitive platform that responds effectively and predictably to pα-Syn concentrations in blood serum. The observed

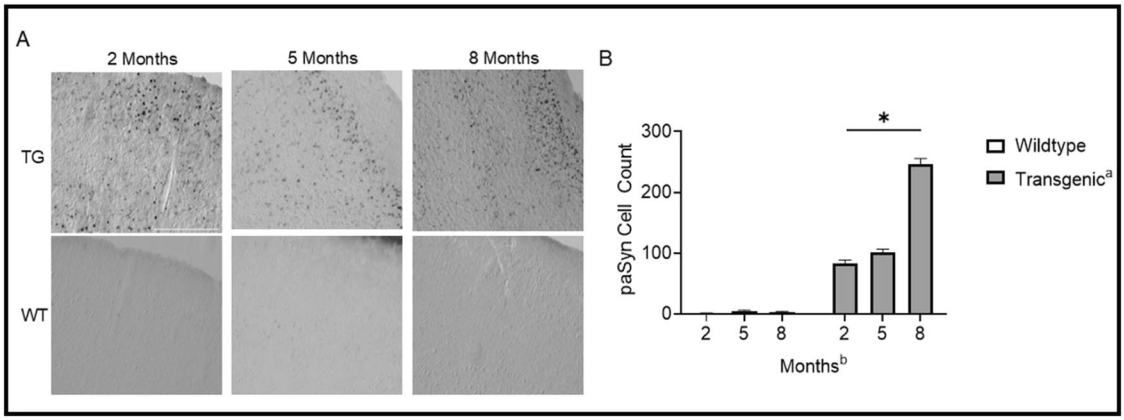

Fig. 8 | Immunohistochemical staining of pα-Syn in the motor cortex of TG and WT mice. A Qualitative representation of pα-Syn-positive cells in the motor cortex of A53T and WT mice. Images taken at 10X magnification. **B** Quantitative summary of pα-Syn-positive cells in 2-, 5-, and 8-month A53T and WT mice. Data are presented as mean ± SEM. The asterisk indicates more pα-Syn staining in the 8-month TG group compared to the 2- and 5-month TG groups, $p < 0.05$. 'a' denotes a significant main effect of genotype (TG vs WT); 'b' denotes a significant main effect of age. Scale bar represents 50 μm.

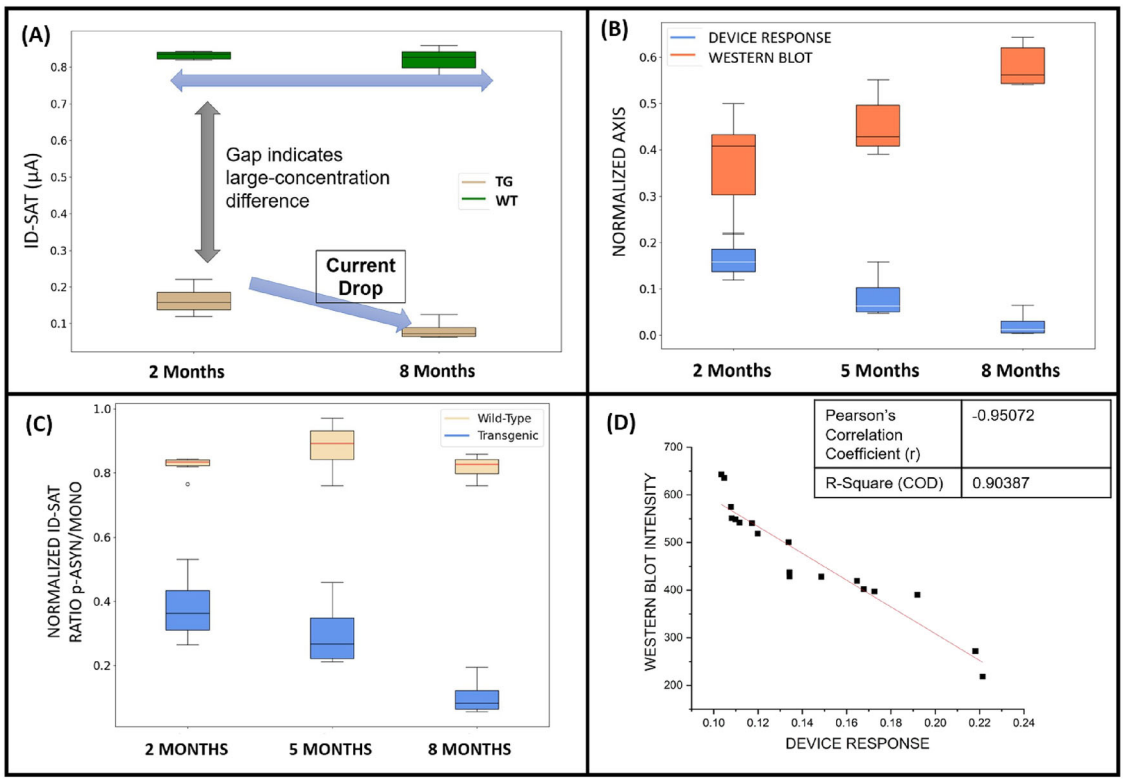

Fig. 9 | Statistical plots for assessing the Ab-OEGFET sensor performance. A Sensor response across longitudinal TG and WT samples. **B** Plot depicting sensor response in comparison with Western Blot. **C** Plot showing sensor current ratio from pα-Syn/mono AB-OEGFET devices. **D** Statistical correlation of Device response vs. Western Blot for pα-Syn concentration in TG model serum samples.

higher range ID-SAT magnitude in WT serum samples and the distinct current drop in TG serum samples with age support the devices' inverse current modulation mechanism. A strong correlation between the 2 quantitative measurements (note that a similar correlation was also observed between the device and immunohistochemistry, a semi-quantitative measure; Supplementary Fig. 10) and further validation reinforces the devices' capacity to track pre-clinical neuropathology associated with PD over time. These findings demonstrate the Ab-OEGFET as a powerful biosensing platform for early-stage detection of changes in toxic forms of α-Syn in neurodegenerative disease models.

Discussion

Novel Organic Electrolyte Gated Transistors with immobilized antibodies (Ab-OEGFET) are demonstrated as a promising biosensor platform for non-invasive detection and monitoring of multiple fluidic biomarkers associated with neurodegenerative diseases, including the early diagnosis of PD. The sensor device leverages the high sensitivity of field-effect transistors (FET) and biocompatibility of soft polymer materials with tunable surface properties, to detect the desired protein biomarkers in complex biological fluids such as serum. The work reports one of the largest pre-clinical animal model studies to date, deploying an

electrolyte-gated transistor biosensor platform for PD biomarkers. It is also the first major disease model investigation using the Ab-OEGFET, where a large number of sensor devices (>150 sensors) were fabricated and tested over a year-long period, investigating more than 60 serum samples, including replicates. The biosensors' ability to detect different formations of α-Syn protein in serum samples collected from the A53T TG mice and comparable age WT mice affirms that the platform is capable of differentiating amongst longitudinal samples from patients in future clinical studies. The study also suggests that the device can be used to predict trends in biomarker concentration changes due to progressing disease pathology or in response to a therapeutic treatment regime. The viability of apta-OEGFET was investigated in the study for future multiplexing possibilities, where aptamers and antibodies can be integrated as recognition molecules on the same device footprint. The validation of Ab-OEGFET sensor response in diluted serum samples with brain tissue-based Western Blot testing confirms that the sensor possesses high enough resolution to detect early disease neuropathology in low-volume blood-based screening assays. The demonstrated high sensitivity and specificity of the Ab-OEGFET positions as a transformative sensing technology for early and non-invasive PD diagnostics and a well-suited platform for implementation in clinical studies targeting blood and saliva biomarker-based monitoring of neurodegenerative disease pathology progression.

Methods

Materials

Polyaniline substrates (500HN Kapton®), provided by Dupont (USA), were used to fabricate all OEGFET devices. Sylgard 184 polydimethylsiloxane (PDMS) was purchased from Dow Chemicals (USA). 6,13-Bis(-triisopropylsilylethynyl) pentacene (TIPS-pentacene), chlorobenzene (PhCl), Poly (vinyl Alcohol) (PVA), A4 950 Poly (methyl methacrylate) (PMMA), (3-Aminopropyl) triethoxysilane (APTES), 1-ethyl-3- (3-dimethylamino) propyl carbodiimide, hydrochloride (EDC), 4-morpholinoethanesulfonic acid (MES), Phosphate buffered Saline (PBS), 2-Mercaptoethanol (ßME), NaCl, N-hydroxysulphosuccinimide (sulpho-NHS) were all purchased from Millipore Sigma (Canada). Anti-α-Syn antibodies – Monomeric total (clone2f12, mAbN1817), Oligomeric total (Sigma Syn33, cat# AbN2265), anti-GFP antibodies (IgY chicken polyclonal, ab13970) were purchased from Millipore Sigma (Canada), whereas anti-phosphorylated α-Syn antibody was purchased from Cell Signaling (cat# 23706). Anti-αSyn aptamers were synthesized by the DeRosa group (LADDER, Carleton University) to investigate for the first time the aptamers' suitability in the biosensor platform for serum biomarker testing.

Gate electrode fabrication

Gate electrodes (50 nm aluminum (Al), 50 nm Chromium (Cr)) were physical vapor deposited (PVD) on Kapton via a stainless-steel shadow mask. PMMA (950k A4; 200 nm) was spin deposited at 4000 rpm and baked at 180°C for 3 minutes. PDMS microchannels (well dimensions 1.5 ×5 mm) were prepared using cured PDMS (375 µm), which were covalently attached using our previously reported low temperature (3- Aminopropyl) triethoxysilane (APTES)-based chemical binding technique[22,34].

Sensor assembly with integrated microchannel

The source-drain (SD) transistor electrodes (channel length, L: 50 µm, aspect ratio (W/L): 50) were deposited using e-beam evaporation (50 nm Al, 50 nm Cr) through shadow mask on a second Kapton substrate (Fig. 1C). TIPS pentacene organic semiconductor (OSC) (1 wt% in PhCl solution at 400 rpm, hot plate annealed at 60°C for 15 minutes, thickness 500 nm) and PVA (2 wt% solution in de-ionized (DI) water at 2500 rpm, thickness 200 nm) were sequentially spun on the SD patterned surface. A 200 nm PDMS layer (spin-coated at 6000 rpm) was deposited on top and cured for 50 minutes at 90°C. Finally, the surface was placed in contact and sealed with the gate microchannel surface after UV functionalizing the second substrate (Fig. 1D, E).

Antibody & Aptamers immobilization

To immobilize the α-Syn Ab following the gate electrode fabrication, the PMMA layer over the substrate was first UV-Ozone activated, followed by the EDC-NHS surface modification process[35]. The substrate was treated for 2 mins with an activation solution (2 mM EDC, 0.1 M MES, 0.5 M NaCl), and Sulpho-NHS (5 mM) was then added to the solution. After 15 min, ßME (5 mM) was added to quench the EDC, and finally the microchannel surface was rinsed with DI water and incubated with 0.4 µL of α-Syn Ab (0.1 mM) for two hours. Antibody immobilization within the microchannel was confirmed through fluorescent microscopy using a hybridization process with its respective fluorescent-tagged secondary antibody. To immobilize the α-Syn-specific aptamer in a separate set of devices, a previously established UV-activation protocol was used[22]. The PMMA layer was UV-activated for 7 minutes and immediately after 10 µL volume of α-Syn specific aptamer solution (concentration: 1 mg/ml) was drop casted over the UV-activated PMMA surface and incubated at room temperature for 2 hours[22]. To validate the successful chemical modification of the PMMA surface and infer aptamer binding, contact angle and surface free energy (SFE) measurements were performed before and after UV activation. A substantial reduction in the contact angle was observed, along with an increase in SFE upon binding. This indicates a significant increase in hydrophilicity that is consistent with the presence of surface-bound aptamers, and the increase in SFE affirms stronger attractive forces on the surface.

Serum sample preparation for device testing

Serum purification was carried out for the collected whole blood samples according to previous protocols[36,37]. Extracted serum samples were subjected to an additional centrifugation process to eliminate residual cell debris. The clarified serum was diluted to prepare a testing solution using 1%PBS and de-ionized water. The serum samples were further diluted in a series pattern to optimize the detection and efficient binding of the target protein biomarker with the respective bioreceptor molecules.

Testing procedure

Device testing was performed by injecting 20 µL of diluted serum sample into the device microchannel (Fig. 9A). The gate and drain terminals were swept in the range of 0 to −2.8 V for V_{GS}, and 0 to −3.5 V for V_{DS} to extract steady-state device output and transfer curves (see Fig. 9E, Fig. 1A, B). Device current was captured using an HP4156A semiconductor parameter analyzer using Keysight Genesis software. The captured raw amperometric data were further analyzed using MATLAB and OriginLab Pro for generating graphical figures and statistical analysis plots. Device data presented as boxplot graphs were first normalized using a consistent baseline established through PBS buffer-only I-V measurements to ensure comparability for statistical analysis. This normalization strategy accounts for device current variations arising from small changes in the crystallinity and grain boundary formation of the Tips-Pentacene semiconductor layer. All boxplot graphs shown in the results section report the mean, interquartile distribution, and outliers for device current in saturation, ID-SAT.

Animals

Breeding pairs were established using 3 WT male mice (cat# 000664) and 3 heterozygous TG female mice (B6; C3-Tg (Prnp-SNCA*A53T) 83Vle/J; cat# 004479) purchased from The Jackson Laboratory, Bar Harbor, ME. The TG mice harbor the A53T human α-Syn gene, *SCNA*, which leads to high levels of p α-Syn[10]. Non-TG (WT) littermates were used as age-matched controls. Mouse DNA was taken from an ear punch and genotyped to validate the genotype. A total of thirty-six mice were used for this study, consisting of 18 WT and 18 heterozygous TG mice. Twelve mice (6 WT and 6 TG), equally divided by sex (3 females and 3 males), were assigned to 3 age groups (2 months, 5 months, and 8 months). Mice were separated according to sex and group-housed in standard polypropylene cages (27 × 21 × 14 cm) and maintained on a 12-hour light/ dark cycle. All procedures were approved by the Carleton University Animal Care Committee in

accordance with the guidelines set out by the Canadian Council for Use and Care of Animals.

Protocols for Anesthesia and Euthanasia: Blood serum and brain sample collection. Mice were anesthetized with a single intraperitoneal injection of Urethane (1.5 g/kg) to induce long-term anesthesia and minimize heart rate variability before terminal blood collection. Deep anesthesia was confirmed through several reflex tests, including toe pinch and blink reflex. Once depth anesthesia was achieved, a midline thoracotomy was performed to expose the heart and major organs. Blood was collected via transcardial puncture by gently inserting a 25-gauge needle attached to a 1 mL syringe into the left ventricle of the heart. Blood was drawn slowly to minimize the risk of hemolysis and prevent the heart from collapsing. A total of 500–800 µL of blood was collected per mouse and immediately transferred to sterile 2 mL microcentrifuge tubes. Samples were left to clot at room temperature (RT) for 30 min before being centrifuged at 1500 g for 15 min at 4°C. The serum supernatant was carefully pipetted into clean microcentrifuge tubes and then stored at -80°C until further use.

Following blood collection, mice were euthanized via transcardiac perfusion with 0.9% sterile saline. A 50 mL Luer Lock syringe (Millipore) fitted with a 25-gauge needle was used to perform the perfusion to clear blood from the brain tissue. The brains were extracted, and one hemisphere was fixed in 4% paraformaldehyde (PFA) in phosphate-buffered saline (PBS) for immunohistochemistry. The other hemisphere was placed on a chilled micro-dissecting block with 0.5 mm slots. Coronal sections of the motor cortex were cut, flash-frozen in sterile microfuge tubes over dry ice, and stored at −80°C for Western blot analysis.

Western blot

Motor cortex lysates were prepared using a RIPA buffer (10 mL 0.01 M PBS containing 10% sodium dodecyl sulfate (SDS), 0.5% sodium deoxycholate, and 1% Triton X-100) mixed with one tablet of complete™ Mini ethylenediaminetetraacetic acid (EDTA)-free protease inhibitor (Roche, Cat # 11836170001).

For Western blotting, 12.5 µg of denatured protein was loaded per lane onto a 12.5% polyacrylamide gel and separated by SDS-PAGE. Proteins were transferred onto a polyvinyl difluoride (PVDF) membrane (0.45 µm pore size, Immobilon-P, Millipore) using a wet transfer system. Membranes were allowed to be air-dried overnight prior to immunoblotting.

To normalize Western blot data, total protein was assessed by using a REVERT total Protein stain. Membranes were rehydrated in methanol for 30 s and transferred to a REVERT total protein solution for 5 mins. Once stained, the membranes were washed (2 × 2 mins) in a REVERT wash solution (6.7% Glacial Acetic Acid, 30% Methanol). After a brief wash of distilled water, membranes were imaged using a LI-COR Odyssey system (ThermoFisher) at 700 nm for 2 mins. Total protein was quantified using the REVERT Total Protein protocol, as described below.

After imaging, membranes were washed in Tris-buffered saline (TBS; pH 7.5; 2 ×5 mins) and blocked in TBS containing 0.5% fish gelatin for 1 hr at RT. Membranes were incubated overnight at 4 °C in a primary antibody solution of either anti-aSyn oligomers (1:1000; Sigma Syn33, cat# ABN2265) or anti-phosphorylated-α-Syn (1:1000; Cell Signaling, cat # 23706) in TBS with 0.05% fish gelatin and 0.1% Tween-20. After primary incubation, membranes were incubated with an infrared conjugate secondary antibody (1:10,000; Rabbit 800, LI-COR) in TBS with 0.5% fish gelatin and 0.01% SDS. Membranes were washed (3 × 5 min) in TBS before protein bands were visualized using a LI-COR Odyssey system (ThermoFisher) at 800 nm wavelength for 6 mins. Blot images were obtained and quantified using a Licor Odyssey system (ThermoFisher).

Protein quantification

Total protein normalization was performed using densitometric analysis in Image Studio Lite 5.2 (LI-COR, USA). Membranes were stained using a REVERT total protein stain, and the signal intensity of each lane was quantified. The lane with the highest total protein signal was designated as the reference lane. Normalization ratios for each sample were then calculated using the following formula:

$$\text{Normalization Ratio} = \frac{\text{Lane Intensity}}{\text{Reference Lane Intensity}}$$

These normalization ratios were applied to the target protein signals to correct for any loading variability across samples.

Immunohistochemistry

Immunohistochemistry was performed similarly as previously described by Maletta et al. [38]. The primary antibody used in this study was anti-phosphorylated-α-Syn (1:1000; Cell Signaling, cat # 23706). Images were obtained at 10X magnification, and cells were manually counted for DAB-positive cells.

Statistical analysis

Statistical analysis for the Blot experiments was performed using GraphPad Prism 8 (GraphPad Software, Inc., La Jolla, CA, USA). Levene's and Shapiro-Wilk tests were performed to evaluate skewness and normality[39]. Western blot experiments were conducted across twelve biological replicates ($n = 6$ wild type; $n = 6$ transgenic) with each sample run in technical duplicates per age group. Immunohistochemistry was performed on twelve biological samples, with two technical replicates analyzed per group. Each animal provided one serum sample, which was subsequently followed to seven serial dilutions. Each experimental set comprises seven dilutions with a buffer control, was tested using 3 to 4 OEGFET devices per animal. Therefore, 18–24 devices were used for testing per age group (2-5-8 months old). In total, approximately 54–72 devices were employed to quantify the monomer-total morphology of the α-synuclein (α-Syn) biomarker using OEGFETs functionalized with anti-monomer α-Syn antibodies. A comparable experimental strategy was applied to evaluate the oligomeric form of α-Syn using a separate batch of OEGFETs functionalized with anti-oligomer-specific α-Syn antibodies, bringing the total number of devices for oligomer detection to 54–72. Additionally, monomer-specific aptamer-functionalized OEGFETs were tested with the same batch of serum samples to allow comparative validation across recognition elements. To quantify phosphorylated monomeric α-Syn, serum samples from 12 animals (WT and TG) were analyzed, requiring an additional 36–48 devices. In total, more than 200 OEGFET devices were utilized across all biomarker targets, supporting the comprehensive pre-clinical evaluation of this novel biosensing platform of Ab-OEGFET for α-Syn biomarker detection.

Statistical significance between groups was determined using a two-way analysis of variance (ANOVA) with the Tukey multiple comparisons test. A p-value < 0.05 was considered statistically significant, as indicated by asterisks ($^*p < 0.05$). Data are presented as mean ± SEM. Comparative statistical analysis was performed between device response and Blot data, as well as immunohistochemistry, using Origin Lab (Origin Lab Corporation, Northampton, MA, USA). To visualize device response and western blot data on the same scale, min-max normalization rescaling was performed. Hence, preserved data re-distribution for both cases. Pearson's Correlation Coefficient (r) was measured to analyze the statistical strength and direction of a linear relationship between variables from two different data systems, ranging from -1 to +1[40]. The Coefficient of Determination (R^2), was also calculated to affirm the predictiveness of the statistical model, with values close to 1 implying a perfect data fit in the regression analysis[41].

Data availability

The raw datasets generated from Ab-OEGFET device testing and the analyzed statistical data are available upon request to the corresponding author.

Code availability

The code used to analyze the data and generate statistical analysis results is available upon request.

Received: 14 May 2025; Accepted: 17 September 2025;
Published online: 07 November 2025

References

1. Sweeney, P. et al. Protein misfolding in neurodegenerative diseases: implications and strategies. *Transl. Neurodegener.* **6**, 6 (2017).
2. Polymeropoulos, M. H. et al. Mutation in the α-Synuclein Gene Identified in Families with Parkinson's Disease. *Science (1979)* **276**, 2045–2047 (1997).
3. Chan et al. Exploring the connection between the gut microbiome and Parkinson's disease symptom progression and pathology: implications for supplementary treatment options. *J. Parkinsons Dis.* **12**, 2339–2352 (2022).
4. Jankovic, J. & Tan, E. K. Parkinson's disease: etiopathogenesis and treatment. *J. Neurol., Neurosurg. Psychiatry* **91**, 795 (2020).
5. Mougenot, A.-L. et al. Prion-like acceleration of a synucleinopathy in a transgenic mouse model. *Neurobiol. Aging* **33**, 2225–2228 (2012).
6. Lee, M. K. et al. Human α-synuclein-harboring familial Parkinson's disease-linked Ala-53 → Thr mutation causes neurodegenerative disease with α-synuclein aggregation in transgenic mice. *Proc. Natl. Acad. Sci.* **99**, 8968–8973 (2002).
7. Martin, L. J. et al. Parkinsons Disease α-Synuclein Transgenic Mice Develop Neuronal Mitochondrial Degeneration and Cell Death. *J. Neurosci.* **26**, 41–50 (2006).
8. Paumier, K. L. et al. Behavioral characterization of A53T mice reveals early and late stage deficits related to Parkinson's disease. *PLoS One* **8**, e70274 (2013).
9. Kawahata, I., Finkelstein, D. I. & Fukunaga, K. Pathogenic Impact of α-Synuclein Phosphorylation and Its Kinases in α-Synucleinopathies. *Int J. Mol. Sci.* **23**, 6216 (2022).
10. Giasson, B. I. et al. Neuronal α-Synucleinopathy with severe movement disorder in mice expressing A53T Human & α-Synuclein. *Neuron* **34**, 521–533 (2002).
11. Bencsik, A., Muselli, L., Leboidre, M., Lakhdar, L. & Baron, T. Early and persistent expression of phosphorylated α-Synuclein in the Enteric nervous system of A53T mutant human α-Synuclein transgenic mice. *J. Neuropathol. Exp. Neurol.* **73**, 1144–1151 (2014).
12. Farrell, K. F. et al. Non-motor Parkinsonian pathology in aging A53T α-Synuclein mice is associated with progressive synucleinopathy and altered enzymatic function. *J. Neurochem.* **128**, 536–546 (2014).
13. Russo, M. J. et al. High diagnostic performance of independent alpha-synuclein seed amplification assays for detection of early Parkinson's disease. *Acta Neuropathol. Commun.* **9**, 179 (2021).
14. Maddocks, G. M., Eisenstein, M. & Soh, H. T. Biosensors for Parkinson's disease: where are we now, and where do we need to go?. *ACS Sens* **9**, 4307–4327 (2024).
15. Sekimori, T., Fukunaga, K., Finkelstein, D. I. & Kawahata, I. Advances in blood biomarkers and diagnosis approaches for neurodegenerative dementias and related diseases. *JIN* **23**, 188 (2024).
16. Wang, C. et al. Point-of-care diagnostics for infectious diseases: From methods to devices. *Nano Today* **37**, 101092 (2021).
17. Guo, L. et al. Electrochemical protein biosensors for disease marker detection: progress and opportunities. *Microsyst. Nanoeng.* **10**, 65 (2024).
18. Torricelli, F. et al. Electrolyte-gated transistors for enhanced performance bioelectronics. *Nat. Rev. Methods Prim.* **1**, 66 (2021).
19. Macchia, E. et al. Ultra-sensitive protein detection with organic electrochemical transistors printed on plastic substrates. *Flex. Print. Electron.* **3**, 034002 (2018).
20. Ricci, S. et al. Label-free immunodetection of α-synuclein by using a microfluidics coplanar electrolyte-gated organic field-effect transistor. *Biosens. Bioelectron.* **167**, 112433 (2020).
21. Tibaldi, A. et al. Electrolyte-gated organic field-effect transistors (EGOFETs) as complementary tools to electrochemistry for the study of surface processes. *Electrochem Commun.* **98**, 43–46 (2019).
22. Massey, R. S. et al. Non-invasive monitoring of α-Synuclein in saliva for Parkinson's disease using organic electrolyte-gated FET Aptasensor. *ACS Sens* **8**, 3116–3126 (2023).
23. Johri, S., Massey, R. S., Chan, D., Holahan, M. R. & Prakash, R. ß -Amyloid as a Novel Target Biomarker for the OEGFET Biosensor, Revolutionizing Noninvasive Alzheimer's Screening. *IEEE Sens Lett.* **8**, 1–4 (2024).
24. Massey, R. S., Johri, S., Chan, D., Holahan, M. R. & Prakash, R. Comparison of Aptamer and antibody bioreceptors in the OEGFET biosensor platform for detecting α-Synuclein, a Parkinson's Biomarker. *IEEE Sens Lett.* **8**, 1–4 (2024).
25. Dovonou, A. et al. Animal models of Parkinson's disease: bridging the gap between disease hallmarks and research questions. *Transl. Neurodegener.* **12**, 36 (2023).
26. Trlin, P. et al. Retinal hyperspectral imaging in mouse models of Parkinson's disease and healthy aging. *Sci. Rep.* **14**, 16089 (2024).
27. McConnell, E. M. et al. Selection of DNA aptamers that prevent the fibrillization of & α-synuclein protein in cellular and mouse models. *Mol. Ther. Nucleic Acids* – 35, (2024).
28. Oaks, A. W., Frankfurt, M., Finkelstein, D. I. & Sidhu, A. Age-dependent effects of A53T Alpha-Synuclein on behavior and dopaminergic function. *PLoS One* **8**, e60378 (2013).
29. Song, D.-Y. & Li, J.-Y. Revisiting the advance of age-dependent α-synuclein propagation and aggregation. *Ageing Neurodegen. Dis.* **5**, (2025).
30. Buchman, A. S. et al. Nigral pathology and Parkinsonian signs in elders without Parkinson disease. *Ann. Neurol.* **71**, 258–266 (2012).
31. Park, M. J., Cheon, S.-M., Bae, H.-R., Kim, S.-H. & Kim, J. W. Elevated Levels of α-Synuclein Oligomer in the Cerebrospinal Fluid of Drug-Naïve Patients with Parkinson's Disease. *J. Clin. Neurol.* **7**, 215–222 (2011).
32. Kumar, S. T. et al. How specific are the conformation-specific α-synuclein antibodies? Characterization and validation of 16 α-synuclein conformation-specific antibodies using well-characterized preparations of α-synuclein monomers, fibrils and oligomers with distinct structures and morphology. *Neurobiol. Dis.* **146**, 105086 (2020).
33. Dent, S. E. et al. Phosphorylation of the aggregate-forming protein alpha-synuclein on serine-129 inhibits its DNA-bending properties. *J. Biol. Chem.* **298**, 101552 (2022).
34. Massey, R. S. & Prakash, R. A low-temperature-processed, soft-fluidic OEGFET Saliva Aptasensor for Cortisol. *IEEE J. Flex. Electron.* **1**, 64–72 (2022).
35. Tsai, T.-C. et al. In situ study of EDC/NHS immobilization on gold surface based on attenuated total reflection surface-enhanced infrared absorption spectroscopy (ATR-SEIRAS). *Colloids Surf. B Biointerfaces* **175**, 300–305 (2019).
36. Argmann, C. A. & Auwerx, J. Collection of Blood and Plasma from the Mouse. *Curr. Protoc. Mol. Biol.* **75**, 29A.3.1–29A.3.4 (2006).
37. Methods of Blood Collection in the Mouse. (2000). *Lab Animal*, **29**, 1–4 (2000).
38. Maletta, T., Palummieri, M., Correa, J. & Holahan, M. R. Preadolescent exposure to a sexually mature, unrelated male rat reduces postadolescent social recognition memory and CA2 c-Fos labeling. *Front. Behav. Neurosci.* 17-2023, (2023).
39. Mishra, P. et al. Descriptive statistics and normality tests for statistical data. *Ann. Card. Anaesth.* **22**, 67–72 (2019).
40. Schober, P., Boer, C. & Schwarte, L. A. Correlation Coefficients: appropriate use and interpretation. *Anesth. Analg.* **126**, 1763–1768 (2018).
41. Chicco, D. W. M. J. G. The coefficient of determination R-squared is more informative than SMAPE, MAE, MAPE, MSE and RMSE in regression analysis evaluation. *PeerJ Comput. Sci.* **7**, e623 7:e623 (2021).

Acknowledgements
The authors are thankful to the Natural Sciences and Engineering Research Council (NSERC) of Canada for the financial support through the Discovery Grant. The authors acknowledge support from Carleton Microfab staff in device fabrication.

Author contributions
S.J., D.C. and R.M. conducted experimental work, S.J. fabricated the biosensor devices used in the study, D.C. and M.R.H. established the A53T mouse model, D.C. collected mouse samples, D.K. and M.C.D. synthesized the aptamer and assisted with the aptamer experiment and data analysis, S.J., D.C., M.R.H. and R.P. wrote the manuscript text and conducted data analysis, and S.J., D.C. and R.M. prepared the manuscript figures. All authors edited the manuscript with editing and revisions.

Competing interests
The authors declare no competing interests.

Additional information
Supplementary information The online version contains supplementary material available at https://doi.org/10.1038/s44328-025-00057-8.

Correspondence and requests for materials should be addressed to Ravi Prakash.